Eur. Phys. J. D **35**, 125–133 (2005)
DOI: 10.1140/epjd/e2005-00177-6

THE EUROPEAN PHYSICAL JOURNAL D

# Long distance magnetic conveyor for precise positioning of ultracold atoms

R. Long[1,2,a], T. Rom[1,b], W. Hänsel[1,c], T.W. Hänsch[1], and J. Reichel[1,2,d]

[1] Max-Planck-Institut für Quantenoptik and Ludwig-Maximilians-Universität München, Schellingstrasse 4, 80799 München, Germany
[2] Laboratoire Kastler Brossel, Département de Physique de l'École Normale Supérieure, 24 rue Lhomond, 75231 Paris Cedex 05, France

Received 2 May 2005
Published online 28 June 2005 – 

**Abstract.** We describe a chip-based magnetic conveyor that transports ultracold atoms with high positioning accuracy over long distances, into an interaction region which is well separated from the magneto-optical trap and gives good optical access to the atoms. The conveyor can work in two different modes, with or without external bias field. The transport potential is generated by a two-layer conductor pattern, enabling a significantly smoother transport than our earlier single-layer conveyor. This is confirmed by numerical field calculations, using an optimization procedure that minimizes shape deformations as well as deviations from the linear transport path. We experimentally demonstrate the use of this conveyor in the mode with external bias field, transporting a cloud of cold atoms over a linear distance of 6 cm and a total distance of 24 cm. We also describe an on-chip quadrupole trap that can be rotated by $\pi/2$. This trap is used to remove design constraints on the orientation of the laser beams in the surface magneto-optical trap. The long-distance conveyor is a versatile tool for experiments with trapped cold atoms, and can achieve sub-micrometric positioning precision. Possible applications of this tool are discussed.

**PACS.** 32.80.Pj Optical cooling of atoms; trapping – 03.75.Be Atom and neutron optics

## 1 Introduction

The production of cold atomic ensembles has been routinely available in laboratories for about two decades. In most cases, the atoms stay localized at the same position, or are launched or simply dropped. Recently, there has been a growing interest to develop techniques for transporting and positioning trapped atom clouds. Such techniques make it possible to deliver cold atoms in a region free of the lasers and coils of a magneto-optical trap, allowing optical and mechanical access. This is a crucial issue for probing a surface or any material structure, for loading atoms in optical lattices, or for positioning atoms in an optical cavity.

One possible technique is the optical dipole trap, which has been used to transport single atoms [1] or Bose-Einstein Condensates [2]. But it requires optical access for the dipole trapping beam and allows a limited range of manipulation. The other possibility is to use magnetic traps. By using macroscopic coils to generate the magnetic field potential, cold atoms have been transported from a MOT-loading region to an optical lattice-loading region [3]. The use of a succession of macroscopic coils allows the transport of a large number of atoms, but increases the size of the set-up.

A more compact approach involves magnetic microtraps [4–6]. Miniaturized conductor patterns on a chip allow the creation of a large diversity of non-periodic, built to purpose magnetic potentials, giving an unprecedented freedom to the experimentalists. Since the first demonstration of a micro-trap [7], a number of different building blocks have been achieved: a conveyor for transporting cold atoms over 4 mm at a speed of about 5 mm/s [8], atom guides [9–11], incoherent spatial beam-splitter [12], switch [13] and the realization of Bose-Einstein Condensation on a chip [14,15]. An optimization of the driving currents and fields even made it possible to transport a BEC over a small distance on the conveyor [14,16].

In order to transport atoms into a freely accessible region, which is unobstructed by MOT beams and coils, we have developed an improved conveyor that combines faster transport over longer distances with high positioning accuracy. Its principle of operation generalizes that of the

[a] *Present address*: Physics Department, Stanford University, Stanford, USA.
[b] *Present address*: Johannes Gutenberg-Universität, Mainz, Germany.
[c] *Present address*: Leopold-Franzens-Universität, Innsbruck, Austria.
[d] e-mail: jakob.reichel@lkb.ens.fr

first-generation device. It allows trapping and transport without external (i.e., coil-generated) fields and with greatly improved smoothness of transport. Technically, these improvements are enabled by the use of a multilayer fabrication technique. A similar approach is described in [6,17]. In the present paper, we describe in Sections 2 and 3 the conception and fabrication of our improved conveyor. In Section 4, we report the $\pi/2$ rotation of an atom cloud around a circular conductor and the realization of an integrated three wire atom guide. In Section 5, we present the transport of an atom cloud over a macroscopic distance of 24 cm, more precisely over two round trips of a 6 cm stroke. We are using this conveyor in an application where trapped atoms are to be coupled to the ultrahigh-finesse modes of a microsphere resonator, requiring an extremely high positioning accuracy. In this application, the conveyor is used to transport the atoms from the magneto-optical trapping region to the microsphere location. However, as we point out in the conclusion, we believe that this long-distance conveyor has the potential to serve in a large variety of applications.

## 2 Long distance magnetic conveyor chip

The basic idea of both the first, single-layer conveyor belt [8,16] and the two-layer conveyor described here is to employ a static 2D quadrupole potential for transverse confinement and to superpose a time-dependent longitudinal potential for transport. The 2D quadrupole is created using one or several guide wires along the transport direction, while the shifting wires run perpendicular to the transport direction, so that their main field component, at the location of 2D quadrupole minimum, is along the transport direction. As this field component is perpendicular to the 2D quadrupole field, it can be modulated without interfering with the transverse confinement. However, in a single-layer structure, the shifting wires must be bent to avoid crossing the guide wire (which would create a short circuit), so that they run parallel to the latter for some fraction of a period. Where they do so, they create a field which does interfere with the 2D quadrupole, leading to a transverse displacement of the trap center. In our first conveyor experiment, which used sinusoidal current modulation, the periodic excursions around the straight-line transport path had an amplitude as large as $\pm 75\,\mu$m [16]; this and an associated "breathing" (variations by a factor $\sim 2$ in the trap frequencies) lead to a heating rate which was measurable when the transport speed $v$ exceeded $\sim 1$ cm/s and depended quadratically on velocity with a constant $4.6\,\mu\mathrm{K}/(\mathrm{cm/s})^2$. Although excursions and breathing could be significantly reduced along a subset of axes by using non-sinusoidal modulation currents and simultaneously modulating all other trapping fields [16], we could not eliminate all position and trap frequency deviations at once. Thus, although we were able to transport transport a BEC on the single-layer conveyor [14], the transport distance was limited to two periods (1.6 mm) and a mean speed of 1.6 cm/s.

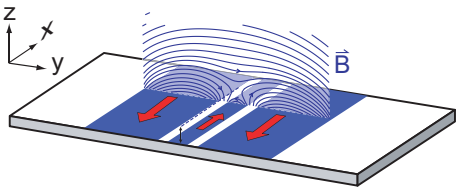


**Fig. 1.** Three-wire pattern providing the transverse confinement. The spacing between the wires is $100\,\mu$m. The width of the central wire is $200\,\mu$m, the width of the outer wires is $750\,\mu$m. To achieve a trap depth of 17 G for a trap-surface distance $z_0 = 120\,\mu$m, the current in the central wire is $I_c = 0.86$ A, and in the left and right outer wires $I_{ol} = I_{or} = -5.3$ A. The magnetic gradient is 1400 G/cm and the dissipated power is 10 W for a length of 72 mm.

To achieve a longer transport (over several cm), the heating rate needs to be reduced significantly because the speed of the transport must be increased in order to circumvent the limitation of the lifetime by background collisions. In this section, we describe the realization of a 10 cm long multilayer chip with six independent conductors performing the shifting of atom clouds. We will detail the chip design for the transverse confinement, the longitudinal confinement and the transport, the procedure to load the atoms, and finally the fabrication of the chip.

### 2.1 Transverse confinement

To transport the atoms in a given direction, we first have to ensure the confinement of the atoms in the transverse plane. This is achieved by an atom guide. In the following, we will denote the transport direction as **x**, the axis orthogonal to the chip surface as **z**, and the remaining axis as **y**. An atom guide is often realized by a wire and a homogeneous field perpendicular to the wire. However, to transport the atoms over a distance of 6 cm, this solution requires very large coils to generate the external field. A more compact solution is suited. Several configurations have been proposed to create integrated atom guides without any additional coils [18] and some of them implemented [9,10,19]. We have chosen the configuration with three parallel wires, which we will call the *guiding wires*. It is the simplest configuration leading to a minimum in the magnetic potential (i.e., a two-dimensional trap) outside the plane containing the wires. The exact design of our implementation is presented in Figure 1. The minimum spacing between the conductors is fixed by the fabrication process at $100\,\mu$m. The other parameters (in particular, the widths of the conductors) are determined by imposing the distance $z_0$ between the trap and the chip surface, by minimizing the ohmic power dissipated, and by maximizing the trap depth, which is the case when the total field modulus has the same value at the central conductor surface and at the local maximum obtained away from the substrate along the $z$-axis (equal barrier heights towards and away from the substrate).

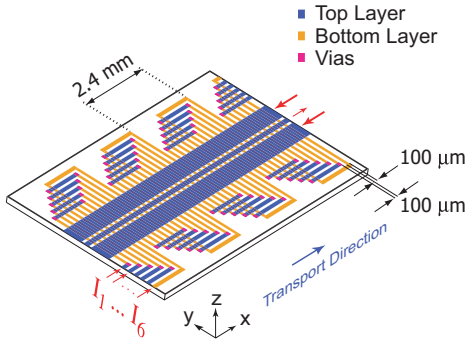


**Fig. 2.** Structure of the multilayer chip. The conductors providing the transverse confinement (cf. Fig. 1) are on the top layer. The six conductors that are responsible for the longitudinal confinement and shifting are on the bottom layer, except for the bridges that enable non-contact crossings. Each bridge consists of a wire section on the top layer and two "vias" providing connections between the layers. The width of the shifting wires as well as the spacing between these wires is determined by the fabrication process to 100 $\mu$m.

### 2.2 Longitudinal confinement and transport

As in the first conveyor [8], the longitudinal confinement is provided by wires perpendicular to the transport direction. In the following, we will refer to these wires as *shifting wires*. There are two ways to obtain this longitudinal confinement. The first is to add a homogeneous longitudinal bias field, in which case the shifting wires are used to reduce the field, creating a minimum in the potential. In the second scheme, trapping wells are created between two potential maxima generated by the shifting wires. In this case, no external fields are required. In both cases, we obtain a chain of magnetic trapping wells, each of which is of the Ioffe-Pritchard type. These wells can be continuously shifted by appropriately modulating the wire currents. To increase the speed of the transport and avoid heating up the trapped atoms, we have to translate the magnetic trap without any deformation of the potential shape, and this translation has to be as close as possible to a uniform movement. To fulfill these requirements, the conductor pattern should be as symmetric as possible. A multilayer substrate offers significant advantages here, as the shifting wires can then cross the guiding wires. In the first conveyor, they had to be bent to avoid the crossing, leading to undesired additional field components [16]. Moreover, using a multilayer pattern, the shifting wires can also cross one another, so that more than two of them may be used. We have chosen to use six independent shifting wires (Fig. 2). Although two conductors are sufficient to achieve transport (as was the case for the first conveyor), we found that a higher number of independent wires is helpful for a smooth transport. In particular, the currents through these wires are additional parameters that can be used to minimize the deviations from the desired longitudinal trap shape during transport, reducing parametric heating.

The width of the shifting wires as well as the gaps between the wires are limited by the fabrication process to 100 $\mu$m. In one period of the conveyor, each of the six shifting wires crosses the transverse-confinement conductors twice (once in the $+\mathbf{y}$-direction and once in the $-\mathbf{y}$-direction). The length of one period is 2.4 mm. Figure 3 shows the finished substrate.

### 2.3 Optimization of the conveyor potential

With the conductor pattern defined above, we have 9 independent currents that need to be optimized to achieve smooth transport. This task is largely simplified by the high degree of symmetry of the conductor pattern. To simplify the discussion, we will not consider the edge effects at the ends of the conveyor in this section (loading will be discussed in the next section). Let us call $I_c$ the current in the central guiding wire, $I_{ol}$ and $I_{or}$ the currents in the outer guiding wires, and $I_1 \ldots I_6$ the currents in the six shifting wires. $\mathbf{B}_g$ denotes the total field of the guiding wires and $\mathbf{B}_s$ that of the shifting wires; field components are denoted $B_{gx}$, $B_{sx}$ etc. The optimization proceeds in three steps.

1. *Transverse potential.* To a good approximation, the transverse potential is determined only by the three guiding wires. To see why this is the case, first note that $\mathbf{B}_g$ is a 2D quadrupole in the $yz$-plane, and is translationally invariant along $x$. In absence of other fields, this quadrupole forms an atom guide along $x$ at some height $z_0$ above the substrate and some transverse position $y_0$, centered above the central guiding wire ($y_0 = 0$) if the outer wire currents are equal, $I_{ol} = I_{or}$. $\mathbf{B}_s$, on the other hand, is in the $xz$-plane (neglecting the bridges, which are located far away). Therefore, any interference between the guiding wire potential and the shifting wire potential can only involve their $B_z$ field components. The effect of $B_{sz}$ is to cause a displacement of the quadrupole, the field in the displaced center still being equal to zero — a well-known effect when one adds a homogeneous field to a quadrupole. If the transverse confinement is much stronger than the longitudinal confinement — which is the case in our conveyor — then this displacement is very small. Thus, by choosing the currents $I_c$ and $I_{ol} = I_{or}$, we fix, to first order, the vertical position $z_0$ of the guide and its transverse gradients, and these parameters will be modified only very slightly by the shifting potential.
2. *Longitudinal potential.* Now we focus on the potential on the guide axis, i.e., on the line $(x, y = 0, z = z_0)$. As mentioned above, $\mathbf{B}_s$ only has components in the $xz$-plane. We have already seen that $B_{sz}$ slightly displaces the guide center (an effect which we address in the next step), but does not change the field in the center. Thus we see that the longitudinal confining potential is simply determined by the field component $B_{sx}$. It is now very simple to numerically optimize the shifting wire currents $I_1 \ldots I_6$ such that the field $|B_{sx}(x, y = 0, z = z_0)|$ approximates some desired longitudinal target potential well $P(x)$. By symmetry,

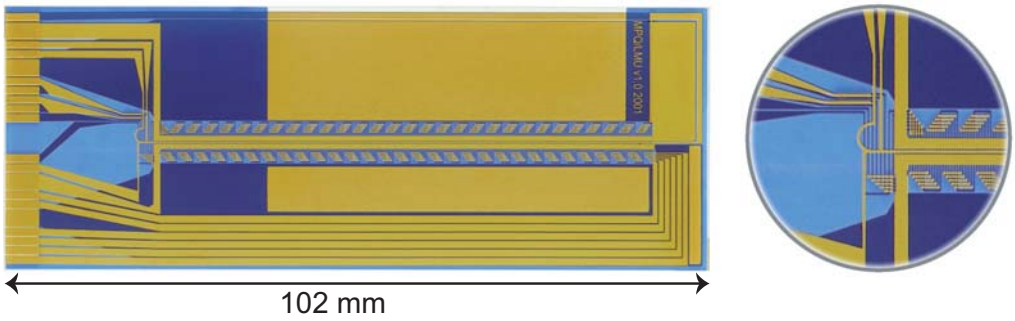


**Fig. 3.** Photograph of the complete substrate before application of the mirror layer. The right panel shows a magnification of the loading region. Note that the base conductor layer shines through the semi-transparent, blue insulation layer.

it is sufficient to do this over one half-period, i.e., over a length $\delta x = 1.2\,\mathrm{mm}$[1].

3. *Correction of the transverse position.* Optionally, the slight lateral displacement caused by $B_{sz}$ can be removed. This is achieved by slightly imbalancing the currents $I_{ol}$ and $I_{or}$ so that their resulting $B_z$ component exactly cancels $B_{sz}$.

The currents resulting from this three-step procedure create a chain of identical potential wells, each of which approximates the shape of the target potential $P(x)$ (displaced by the appropriate number of periods). The goal is now to maintain the shape of these wells while translating them along the transport direction. This is achieved by incrementally displacing the target potential, each time performing steps 2 and 3 again to calculate the appropriate currents. As before, it is sufficient for the optimization to consider a single well in the chain. For concreteness, let us define $P(x)$ so that it has its minimum at $x = 0$. Also, let us call $P_{x_c}(x) = P_x(x - x_c)$ the target potential which has been translated so that its minimum is located at $x_c$. Performing steps 2 for a particular $x_c$ provides us with the currents $I_1(x_c) \ldots I_6(x_c)$ that must be applied in order to obtain the best approximation to the displaced longitudinal potential $P_{x_c}(x)$. The procedure is repeated for increasing values of $x_c$, yielding current modulation functions $I_1(x_c) \cdots I_6(x_c)$ for the complete range of $x_c$. (Further exploiting the symmetry, the problem reduces to optimizing the translation of the potential from one shifting wire half-way to the next, i.e. over a distance $\Delta x = 100\,\mu\mathrm{m}$ for our conductor and gap widths.) In the experiment, $x_c$ is a function of time, $x_c(t)$, and so are the currents: $I_1(x_c(t)) \cdots I_6(x_c(t))$.

We have implemented this optimization procedure using Biot-Savart type calculations that take into account the width of the conductors. Figure 4 shows the initial potential, which is created by the currents indicated in the figure. This potential was also used as the target potential

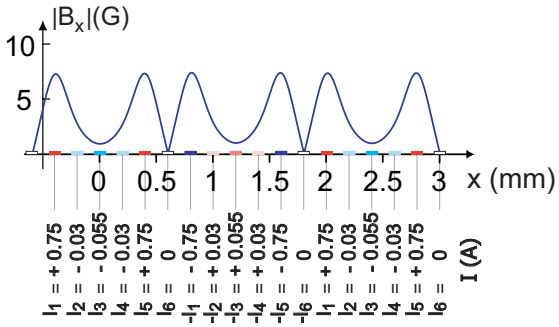


**Fig. 4.** Potential along the transport direction for a conveyor without external field. The rectangles on the $x$-axis represent the shifting conductors (to scale). The potential is created by the currents indicated below the wires. This potential was used as the target potential in the numerical optimization of the transport. Its trapping frequencies are 92 Hz longitudinally and 1.8 kHz transversally, for the $^{87}$Rb $F = 2, m = 2$ state used in the experiment.

in the optimization. (Thus, the deviation from the target potential is 0 for $t = 0$ by construction.) Having obtained the current modulation functions, we have cross-checked the result by performing a three-dimensional Biot-Savart calculation with the full conductor pattern (including, for example, the bridges) and all field components. The deviation of the trap center trajectory from a straight linear transport path was smaller than 30 nm at all times[2]. When we omitted step 3 of the optimization procedure (i.e., no modulation of the outer guiding wires), the deviation of the trap center trajectory still remained smaller than 10 $\mu$m at all times. These results confirm a posteriori the validity of the approximations used in the optimization procedure, and demonstrate the power of the multilayer conveyor scheme. In the experiment, the final accuracy will no longer be limited by the transport scheme itself, but only by fabrication tolerances in the conductor pattern and by magnetic noise from the current sources and from the background magnetic field in the lab [16].

[1] Additionally, a weighting function can be used when evaluating the deviation from the target potential. For a hot thermal cloud, the deviation should be minimized over the full extent of the potential well. For transporting a BEC, only the central part of the potential is relevant and should receive a higher weight in the optimization, further reducing the deviation in that region.

[2] The value of this deviation also depends on the weighting function (see previous footnote). Here we have chosen to minimize deviation over a large spatial extent of $\delta x = 750\,\mu\mathrm{m}$ because the goal was to transport a thermal cloud.

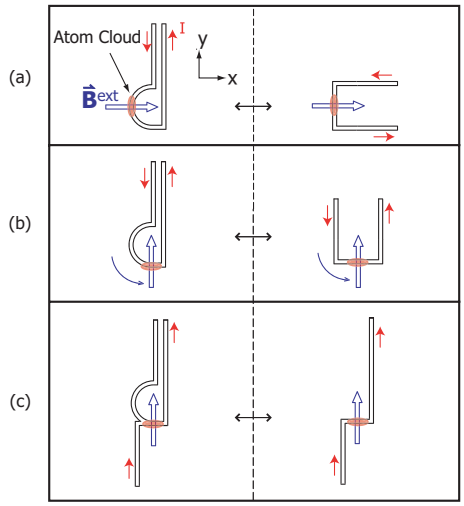


**Fig. 5.** Different phases of the atom loading into the conveyor, with the real conductor pattern (left column) and its analog in terms of "standard" micro-trap conductors (right column). (a) Loading into the initial quadrupole trap from a "U"-shaped conductor which is also used for the mirror-MOT. (b) The quadrupole trap cloud is turned by $\pi/2$ by rotating the external magnetic field. (c) Transfer into an Ioffe-Pritchard trap created by a "Z"-shaped conductor.

### 2.4 Loading atoms in the conveyor: rotatable quadrupole trap

To load cold atoms into the chip trap, we use a mirror-MOT [7], which involves only four beams, two of the beams being reflected by a silver layer on top of substrate. This procedure usually involves two steps. First, a MOT is obtained with the quadrupole field of external anti-Helmoltz coils, which gives a large capture volume and so a large number of atoms. Then the MOT is shifted towards the surface of the chip, and the quadrupole field of the coils is replaced by the quadrupole field generate by a "U"-shape conductor on the chip. An efficient transfer mechanism is then realized between the MOT and the magnetic trap, by simply switching off the lasers. Here, however, we obtain after this sequence a cigar-shaped cloud on the axis of the central wire of the "U" (i.e. the **y**-axis), which is also the direction of propagation of the two MOT-beams parallel to the chip. But for the transport, the long axis of the cloud must be the direction of the transport — which can only be the **x**-axis because we want to transport the atoms out of the region illuminated by the MOT beams. Thus, in order to obtain a good mode matching between the MOT and the magnetic trap at the starting position of the conveyor, we have to invert the aspect ratio of the atom cloud. We do this by simply turning the cloud, using a novel "P"-shaped conductor (see Fig. 5) instead of the traditional "U". With this conductor, a quadrupole trap can be produced for a wide range of orientations of the homogeneous external field $B^{\mathrm{ext}}$. Rotating this field in the $xy$-plane rotates the trap, with the trap center describing a circular path with the same radius as the circular part of the "P". In our implementation, this radius is 1 mm, the conductor width is 200 $\mu$m, and we apply a field $\mathbf{B}^{\mathrm{ext}}(\varphi) = B^{\mathrm{ext}}\big(\cos(\varphi), \sin(\varphi), 0\big)$ with $\varphi = 0 \rightarrow \pi/2$ by using two orthogonal sets of Helmoltz coils (Fig. 5). At the end of the rotation, the atoms are located above a "Z"-shaped conductor so that they can be transferred into a Ioffe-Pritchard (IP) trap by a simple switching of currents. The IP trap allows for evaporative cooling, increasing the phase-space density of the atomic ensemble that is then transported with the conveyor.

## 3 Chip fabrication and experimental set-up

### 3.1 Fabrication of the chip

The first evident feature of this chip is its size. The substrate is a 250 $\mu$m thick, 38 mm × 101.6 mm large aluminium oxide substrate. Our chip has been fabricated at the Max-Planck-Institut für Physik in Munich using thick-film hybrid technology. This is an interesting fabrication process, mainly employed in high-power electronics, which is based on screen printing with metallic and dielectric printing pastes. The desired structure is lithographically transferred to a fine-gauge printing mesh. The printing paste is then squeezed through this mesh onto the substrate. Large-format substrates and thick conductor layers with high current capability are standard with this technology, but the minimum feature size, being limited by the mesh and by the granularity of the printing paste, is not as small as in direct lithographic techniques. In our case, the minimal conductor width was 100 $\mu$m. Our multilayer structure is fabricated in four successive screen-printing steps:

- the bottom conductive layer is applied;
- an insulating layer is applied. This layer has holes at the via positions;
- the holes are then filled with a conductive paste to ensure inter-layers connections;
- finally, the top conductive layer is applied.

After each step, the substrate is baked out at 850 °C to anneal the new conductive or insulating layer and drive out solvents. We have examined the finished substrate under an optical microscope. The conductors are slightly larger than their design size, and graininess is clearly visible on the conductor edges. For the central conductor of the guide (design width 200 $\mu$m), we have measured an actual width between 210 and 220 $\mu$m. The thickness of the conductive layers is about 15 $\mu$m, leading to a relatively low resistance of the shifting wires (total length per wire up to 0.4 m) of around 20 $\Omega$.

The substrate is then glued to a copper block with a thermally conductive glue (Epo-Tek H77). On the atom side of the chip, a silver mirror is glued (Epo-Tek 353ND) by replica technique [20] onto the mirror-MOT loading region. The mirror surface is spaced about 15 $\mu$m from the top surface of the conductors.

The finished chip is connectorized by soldering aluminium connectors on the conductor pads on the chip.

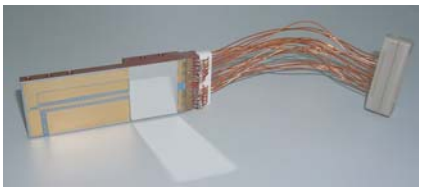

**Fig. 6.** The 10 cm-chip for the long distance transport with the silver mirror covering the MOT-loading region and the connector for the electrical connections.

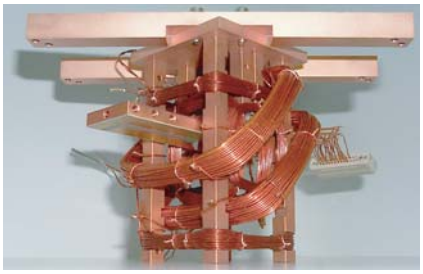

**Fig. 7.** The whole system with the 10 cm-chip mounted horizontally, the coils centered on the MOT-loading region and the freely accessible target region at the end of the conveyor.

Kapton-insulated wires are then soldered onto these connectors. These wires are glued in a Macor piece to relieve stress on the soldered connections. Finally, all the wires are connectorized by a UHV-compatible D-Sub 25 connector, which allows a reliable and easy way to connect and disconnect the substrate to the electrical feed through inside the vacuum chamber (see Fig. 6).

### 3.2 Experimental set-up

The chip assembly is screwed into a copper structure which supports the coils used to create the three orthogonal homogeneous magnetic fields and the magnetic gradient for the first phase of the mirror-MOT (see Fig. 7). These coils are wound using Kapton-insulated wires. At the end of the conveyor, a microsphere cavity set-up is fixed, where the atoms will be transported [21] (not shown in the photograph).

The whole system is then screwed into the vacuum chamber by two copper rods. The 20 l stainless-steel vacuum chamber is pumped by a 400 l/s turbo-molecular pump and a titanium sublimation pump, allowing us to reach a pressure of $3 \times 10^{-10}$ mbar after moderate bake-out, and after carefully degassing the coils and the rubidium dispenser, that we use as rubidium source. Our laser-system is a standard system to achieve a MOT (40 mW cooling light in master-slave configuration, 7 mW repumping light). The Rb-dispenser is placed at 5 cm from the MOT center.

### 3.3 Cold atom preparation

A steady current of 2.5 A is sent through the dispenser, keeping it heated but below the release temperature, and we pulse an additional 5.5 A for 4 s during the 6 s loading phase of the mirror-MOT [22]. This allows us to increase the Rb-pressure during the MOT phase without compromising the lifetime in the magnetic trap. The typical number of $^{87}$Rb atoms in the MOT is $1.5 \times 10^6$.

After a 3 ms molasses cooling phase and an optical pumping pulse, the atoms are transferred into the initial magnetic quadrupole trap. The current flowing in the "P"-shaped conductor is 2.5 A and the external homogeneous field $B_x^{\text{ext}} \simeq 9$ G. We obtain a typical number of atoms in the magnetic trap of $1.1 \times 10^6$ at a temperature of 65 $\mu$K.

## 4 Preliminary experiments

### 4.1 Quadrupole trap rotation

As explained in Section 2.4, we rotate a magnetic quadrupole trap to achieve mode-matching between the MOT and the conveyor potential. The 9 G homogeneous magnetic field is turned by $\pi/2$ in 100 ms. This corresponds to a curvilinear speed of 1.6 cm/s. We have observed for this speed neither losses nor heating of the atoms. For higher rotational speed, losses appear, which may be due to the shape deformation of the potential along the turn[3]. In Figure 8, are represented absorption images of the atom cloud along two orthogonal detection axes, showing the rotation of the cigar-shaped cloud along the circular conductor. We find a good agreement between the calculated position of the cloud and the measured one. At the end of the turn, we obtain a cigar-shaped cloud along the transport direction, ensuring a good mode matching with the conveyor potential.

This atom cloud turning scheme represents a very simple way, just involving one "P"-shaped conductor and two sets of Helmotz coils, to rotate a cloud, solving the problem of mode-matching between the mirror-MOT and the conveyor. It can also by itself be used to transport cold atoms from a MOT-loading region to an interaction region, simply by increasing the size of the radius. For example, a radius of 2 cm is enough to leave a typical MOT-loading region, and the rotation of the cloud can be realized in less than 2 s.

### 4.2 Atom guide

After the turn of the atoms, we obtain a cigar-shaped cloud oriented in the transport direction. We have first checked the transverse confinement of the atoms by releasing them into the guide obtained by powering up the three parallel wires, as described in Section 2.1 (Fig. 9). The current is switched from the "P"-shaped conductor to the central conductor of the three-wires guide, coming from the arc of the "P" conductor. At the beginning,

[3] An accelerating phase at the beginning and a decelerating phase at the end of the turn does not significantly reduce the losses.

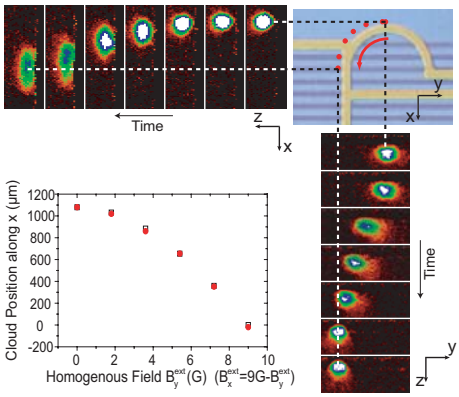


**Fig. 8.** Rotating a trapped atom cloud. The photograph (top, right) shows the relevant part of the conductor pattern. Absorption images were taken with two cameras along two perpendicular axes parallel to the substrate. They are shown in the same scale as the wire pattern. The quadrupole trap is rotated along a 1 mm radius arc in 100 ms by rotation of a 9 G external magnetic field. The current flowing in the "P"-shaped conductor is 2.5 A. The measured positions of the center of the trap (red dots) are in good agreement with the calculated ones (black squares).

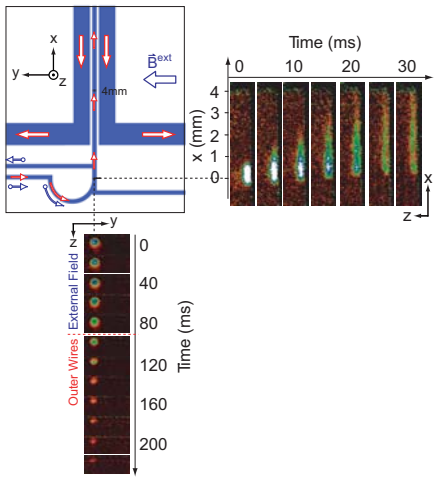


**Fig. 9.** Atom guide. The atoms are released in the guide by changing the current flow. The blue arrows (with circle at end) represent the current flow for the 3D quadrupole trap, the red arrows show the current flow for the atom guide. At the beginning, we use an external magnetic field to obtain the transverse confinement. After 100 ms, we replace it by sending a current through the outer wires, realizing an integrated atom guide without external fields. At the beginning of the release, as the atom cloud spreads along the detection axis, some of the atoms move beyond the initial detection region. As a result the magnetic field applied to define the quantization axis is not constant along the whole extent of the cloud, thus the probe beam is not resonant for all the atoms, leading to an apparent decrease of the number of detected atoms. Real loss occurs towards the end of the sequence, when the fastest atoms drop out of the guide at the end of the chip (a situation that no longer occurs once the shifting potential is added).

the transverse confinement is provided by the central conductor and the external magnetic field already used for turning. Then, when the atoms have reached a position sufficiently far away from the beginning of the outer wires (i.e. after 4.5 mm from the final point of the turn), we switch off the external magnetic field and send a current through the outer wires. The atoms are pushed out into the guide by the magnetic gradient created by the current flowing into the arc of the "P", which is connected in series with the central wire.

## 5 Long distance conveyor

Due to limitations of our current sources, we could only use a maximum current of 0.45 A for the shifting wires when these experiments were performed. For this maximum current, the trap depth is 2 G when the conveyor is used in the configuration described in Section 2.2. In order to increase the trap depth, we have chosen to work with a different configuration of the conveyor, where an external magnetic field parallel to the transport direction is added. In this configuration, the magnetic field created by the shifting wires adds to or subtracts from the homogeneous field, depending on the position in the conveyor. This configuration necessitates the addition of a bias coil at the end of the substrate, which can be tolerated in our application, and increases the trap depth up to about 8 G. Again, we have performed a numerical optimization of the transport with this longitudinal field. The resulting magnetic potential along the transport direction is shown in Figure 10. The calculated transverse trap frequency is 1221 Hz and the longitudinal one 98 Hz. In this configuration, we obtain a better translation of the potential if the atoms are at a distance of 190 $\mu$m from the surface of the chip, where the atoms see the magnetic field of a higher number of shifting wires. This distance is obtained for a current of 1.4 A in the central wire and of 4.5 A in the outer wires. The longitudinal magnetic field is created by the two Helmoltz coils centered on the MOT-loading region and an additional coil positioned at the end of the conveyor chip. These 3 coils are connected in series, and during the displacement of the atoms the current is modified so that the field produced by the coils at the location of the atoms has a constant value of 8 G.

After the turn of the cloud, we transfer the atoms from the quadrupole trap to the Ioffe-Pritchard trap created by the "Z"-shaped conductor with a 9 G homogeneous bias field and a current of 2.5 A. We compress this trap by increasing the bias field to 16 G. Then, we make the current flow through the central wire and we switch on the current of the six shifting wires and the 8 G longitudinal magnetic field. The atoms are then transported over an initial 4.4 mm in 200 ms to reach the region where we can switch off the transverse magnetic field and power up the outer wires. At this point, the atoms are ready to enter the long distance conveyor. During the transfer and the first 200 ms in the transport potential, 2/3 of the atoms are lost, and we usually start the long distance transport

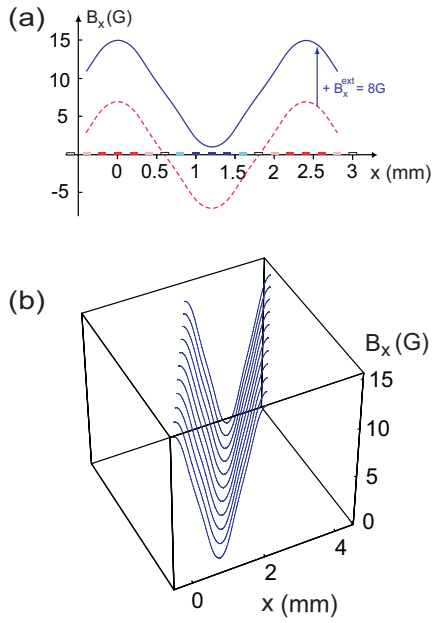


**Fig. 10.** (a) Potential for a conveyor with an external longitudinal field $B_x^{\text{ext}} = 8\,\text{G}$ (cf. Fig. 4). The dashed curve shows the $B_x$ component of the wires alone, the solid curve shows the total $B_x$ field (wires and external field). (b) Calculated potential during transport, with a numerically optimized modulation current function of the shifting wires. The third axis corresponds to time (or phase, as speed is constant) during one conveyor period of 2.4 mm.

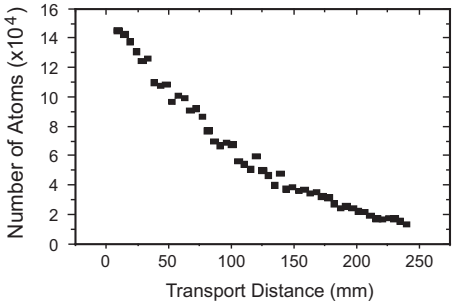


**Fig. 11.** Transport of a cloud of $1.5 \times 10^5$ atoms over about 24 cm (two round trips of a 6 cm stroke) in 2.9 s at an average speed of 8 cm/s.

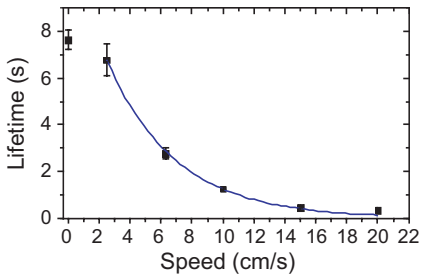


**Fig. 12.** Lifetime of the atoms in the transport potential vs. the speed of the transport.

with $1.5 \times 10^5$ atoms. We have not yet investigated the cause of this loss. One possible reason is the deformation of the transport potential by the conductor along $y$ which connects to the central wire of the three-wire guide. In that case, the problem could be easily solved in a further version of the chip by making this central wire extend beyond the "P" and adding a connecting wire in that region, where it does not interfere with the conveyor potential.

As the detection region in our set-up is limited to the first 5 mm of the transport direction, it is not possible to detect the atoms along the whole transport length. To make measurements for longer transport distances, we reverse the direction of the transport after the first half of the distance. Thus, we detect the atoms when they reenter the detection region after a "return trip". By making two return trips over the full length of the conveyor, we could achieve an atom cloud transportation over 23.5 cm in 2.9 s, at an average speed of $\bar{v} = 8\,\text{cm/s}$. This speed is one order of magnitude above that of the first conveyor. For such a speed, it is important to implement an accelerating phase at the beginning of each trip and a decelerating phase at the end. These phases are usually realized on 2 periods of the conveyor, i.e. on 4.8 mm.

Figure 11 shows the number of atoms as a function of transport distance for $\bar{v} = 8\,\text{cm/s}$. The lifetime of the atoms in the transport trap depends on the speed of the transport. For a static trap, identical to the transport potential, the lifetime is $(7.65 \pm 0.40)\,\text{s}$, limited by collisions with the residual gas at a pressure of $5.6 \times 10^{-10}\,\text{mbar}$. In Figure 12, the lifetime during the transport is plotted for different speeds. For a speed of 2.5 cm/s, it is close to the lifetime obtained for a static potential. For higher speed, the lifetime $\tau$ decreases exponentially, $\tau(v) \propto \exp(-\bar{v}/v_e)$, with a decay constant $v_e = 4.5\,\text{cm/s}$. If we consider the number of atoms vs. the distance they have been traveling, the increase in speed compensates the smaller lifetime for speeds up to 6 cm/s. In the goal to transport atoms to the opposite end of the chip, a trade-off has to be found between a slow transport with losses essentially due to the collisions with the background gas and high-speed transport with losses due to the transport itself.

The losses in this experiment are probably due to residual accelerations of the potential during the translation from one shifting wire to the next. To simplify current control, the currents in the outer wires of the three-wire guide were not modulated in this experiment. The numerical simulations indicate that the center of the potential is shifted laterally by $\pm 1$ $\mu$m along the **y**-axis. In the experiment, there are also deviations of the microfabricated conductor positions and widths from their ideal values, as described in Section 3.1. Although all of these displacements remain small compared to the size of the atom cloud, the resulting accelerations are applied many times: 6 cm transport length corresponds to 26 periods of the conveyor, i.e. more than 300 wire crossings. Therefore, we expect lower heating rates in a substrate fabricated with better precision (for example, standard lithography and evaporation instead of screen printing).

## 6 Conclusion

In this work we have presented an "atom chip" optimized for transportation of ultra cold atoms over distances of several centimeters combined with a high positioning accuracy. This offers perspectives in a variety of applications. As is characteristic of atomic microcircuit devices, it transforms the usual dropped or launched atom cloud into a versatile, highly modulable source of cold atoms. This long-distance conveyor offers a compact and robust way to spatially separate the cold-atom production region — where resonant laser beams and relatively high thermal gas pressures are inevitable — from the interaction region, where sensitive experiments can be performed in an undisturbed environment with good optical access. Compared to coil-based transport [3], it has a complementary set of features: the conveyor is much more compact, has a much lower power consumption, and is easily compatible with other atom chip devices; however, it does not provide the very high average atomic flux that has been achieved with coil-based transport. Thus, we expect its use in precision applications where, typically, a small thermal atom cloud or condensate is needed in a protected environment, and must be positioned with high accuracy. This notably includes the use of atomic samples as probes for surface effects [23], magnetic potential roughness due to geometric fluctuations of wire edges [24–26], or electrical forces [27]. But its functionality can also be used where trapped atoms need to be coupled with an optical cavity [21,28], currently a very active field of research.

In another area, the technique presented here can be readily transposed to the transport and position control of magnetic microbeads commonly used in biotechnology [29,30]. This can allow the control of chemical or biological reactions at the bead surface. These microbeads can also be selectively attached to biological cells, which could then be manipulated [31].

We thank M. Reitmeier and M. Wenninger (Max-Planck-Institut für Physik, München) for the fabrication of the chip. This work was supported by the E.U. under grants IST-2001-38863 (ACQP) and MRTN-2003-505032 (Atom Chips), and by the *Kompetenznetzwerk Quanteninformation* ("A8") of the Bavarian government.

## References

1. S. Kuhr, W. Alt, D. Schrader, M. Muller, V. Gomer, D. Meschede, Science **293**, 278 (2001)
2. T.L. Gustavson, A.P. Chikkatur, A.E. Leanhardt, A. Görlitz, S. Gupta, D.E. Pritchard, W. Ketterle, Phys. Rev. Lett. **88**, 020401 (2002)
3. M. Greiner, I. Bloch, T.W. Hänsch, T. Esslinger, Phys. Rev. A **63**, 031401 (2001).
4. J. Reichel, Appl. Phys. B **75**, 469 (2002)
5. R. Folman, P. Krüger, J. Schmiedmayer, J. Denschlag, C. Henkel, Adv. At. Opt. Mol. Phys. **48**, 263 (2002).
6. J. Fortágh, S. Kraft, A. Günter, C. Trück, P. Wicke, C. Zimmermann, Opt. Commun. **243**, 45 (2004)
7. J. Reichel, W. Hänsel, T.W. Hänsch, Phys. Rev. Lett. **83**, 3398 (1999)
8. W. Hänsel, J. Reichel, P. Hommelhoff, T.W. Hänsch, Phys. Rev. Lett. **86**, 608 (2001).
9. D. Müller, D.Z. Anderson, R. Grow, P.D.D. Schwindt, E.A. Cornell, Phys. Rev. Lett. **83**, 5194 (1999)
10. N.H. Dekker, C.S. Lee, V. Lorent, J.H. Thywissen, S.P. Smith, M. Drndić, R.M. Westervelt, M. Prentiss, Phys. Rev. Lett. **84**, 1124 (2000).
11. A. Leanhardt, A. Chikkatur, D. Kielpinski, Y. Shin, T. Gustavson, W. Ketterle, D. Pritchard, Phys. Rev. Lett. **89**, 040401 (2002)
12. D. Cassettari, B. Hessmo, R. Folman, T. Maier, J. Schmiedmayer, Phys. Rev. Lett. **85**, 5483 (2000).
13. D. Müller, E.A. Cornell, M. Prevedelli, P.D.D. Schwindt, Y.-J. Wang, D.Z. Anderson, Phys. Rev. A **63**, 041602(R) (2001).
14. W. Hänsel, P. Hommelhoff, T.W. Hänsch, J. Reichel, Nature **413**, 498 (2001)
15. H. Ott, J. Fortagh, G. Schlotterbeck, A. Grossmann, C. Zimmermann, Phys. Rev. Lett. **87**, 230401 (2001)
16. P. Hommelhoff, W. Hänsel, T. Steinmetz, T. Hänsch, J. Reichel, New J. Phys. **7**, 3 (2005).
17. A. Günter, M. Kemmler, S. Kraft, C.J. Vale, C. Zimmermann, J. Fortágh, e-print `arXiv:cond-mat/0504209` (2005)
18. J.H. Thywissen, M. Olshanii, G. Zabow, M. Drndić, K.S. Johnson, R.M. Westervelt, M. Prentiss, Eur. Phys. J. D **7**, 361 (1999)
19. R. Folman, P. Krüger, D. Cassettari, B. Hessmo, T. Maier, J. Schmiedmayer, Phys. Rev. Lett. **84**, 4749 (2000).
20. J. Reichel, W. Hänsel, P. Hommelhoff, T.W. Hänsch, Appl. Phys. B **72**, 81 (2001)
21. R. Long, T. Steinmetz, P. Hommelhoff, W. Hänsel, T.W. Hänsch, J. Reichel, Phil. Trans. R. Soc. Lond. A **361**, 1375 (2003)
22. J. Fortagh, A. Grossmann, T.W. Hänsch, C. Zimmermann, J. Appl. Phys. **84**, 6499 (1998)
23. Y.-J. Lin, I. Teper, C. Chin, V. Vuletic, Phys. Rev. Lett. **92**, 050404 (2004)
24. J. Fortagh, H. Ott, S. Kraft, C. Zimmermann, Phys. Rev. A **66**, 041604(R) (2002)
25. A.E. Leanhardt, Y. Shin, A.P. Chikkatur, D. Kielpinski, W. Ketterle, D.E. Pritchard, Phys. Rev. Lett. **90**, 100404 (2003).
26. J. Estève, C. Aussibal, T. Schumm, C. Figl, D. Mailly, I. Bouchoule, C.I. Westbrook, A. Aspect, Phys. Rev. A **70**, 043629 (2004).
27. J.M. McGuirk, D.M. Harber, J.M. Obrecht, E.A. Cornell, Phys. Rev. A **69**, 062905 (2004)
28. P. Horak, B.G. Klappauf, A. Haase, R. Folman, J. Schmiedmayer, P. Domokos, E. Hinds, Phys. Rev. A **67**, 043806 (2003)
29. T. Deng, G.M. Whitesides, M. Radhakrishnan, G. Zabow, M. Prentiss, Appl. Phys. Lett. **78**, 1775 (2001)
30. A. Rida, V. Fernandez, M.A.M. Gijs, Appl. Phys. Lett. **83**, 2396 (2003)
31. H. Lee, A.M. Purdon, R.M. Westervelt, Appl. Phys. Lett. **85**, 1063 (2004)